Scaling approximation for the elementary diagrams in hypernetted-chain calculations

Q. N. Usmani,* B. Friedman, and V. R. Pandharipande
Department of Physics and Materials Research Laboratory, University of Illinois at Urbana-Champaign, Urbana, Illinois 61801
(Received 20 August 1981)

A simple method to sum elementary diagrams in the calculation of two-body and three-body distribution functions by the hypernetted-chain method is proposed. The method is based on the observation that the sum of the elementary diagrams has approximately the same spacial behavior as that of the lowest-order four-body elementary diagram. Thus the sums of two-point and three-point elementary diagrams may be approximated by a scaling constant times the lowest-order contribution. The scaling factor is determined by equating energies calculated with the Jackson-Feenberg and Pandharipande-Bethe expressions. Results of calculations of the energies and distribution functions of liquid ^{4}He with the use of this method are reported. The results obtained with the McMillan correlation function are in almost exact agreement with the Monte Carlo results. Calculations with optimized correlation function having r^{-2} tails are also reported.

I. INTRODUCTION

The problem of calculating the binding energy of liquid ^{4}He starting from a strong two-body interaction is more or less resolved with the Green's-function Monte Carlo (GFMC) method.[1] The main structure of the ground-state wave function is also understood from recent variational Monte Carlo[2] (MC) and hypernetted-chain[3] (HNC) calculations using products of two- and three-body correlations. However, there are still open problems in treating the long-range tails, r^{-2} of the two-body correlation and possibly r^{-3} of the three-body correlation. These tails are particularly important if one wants to obtain a consistent description of the ground state and the low-lying excited states such as phonons, maxons, and rotons, of the liquid.[4] The main object of the present work is to develop methods, within the hypernetted-chain scheme, to treat the long-range pair (or Jastrow) correlations $f(r)$.

The two-particle distribution function $g(r)$, for a Jastrow wave function

$$\Psi = \prod_{i<j} f(r_{ij}) \ , \tag{1.1}$$

is given by[5]

$$g(r) = f^2(r) \exp[N(r) + \epsilon(r)] \ . \tag{1.2}$$

Here $N(r)$ is the sum of nodal diagrams

$$N(r_{12}) = \rho \int [g(r_{13}) - 1][g(r_{23}) - 1 - N(r_{23})] d^3r_3 \tag{1.3}$$

and $\epsilon(r)$ represents the sum of elementary diagrams.

In the HNC method the $\epsilon(r)$ is expanded in a series

$$\epsilon(r) = \epsilon_4(r) + \epsilon_5(r) + \cdots \tag{1.4}$$

and the diagrams that contribute to ϵ_4 and ϵ_5 are shown in Fig. 1. The lines in these diagrams represent $g-1$, thus

$$\epsilon_4(r_{12}) = \tfrac{1}{2}\rho \int [g(r_{13}) - 1][g(r_{23}) - 1][g(r_{14}) - 1] \times [g(r_{24}) - 1][g(r_{34}) - 1] d^3r_3 d^3r_4 \ . \tag{1.5}$$

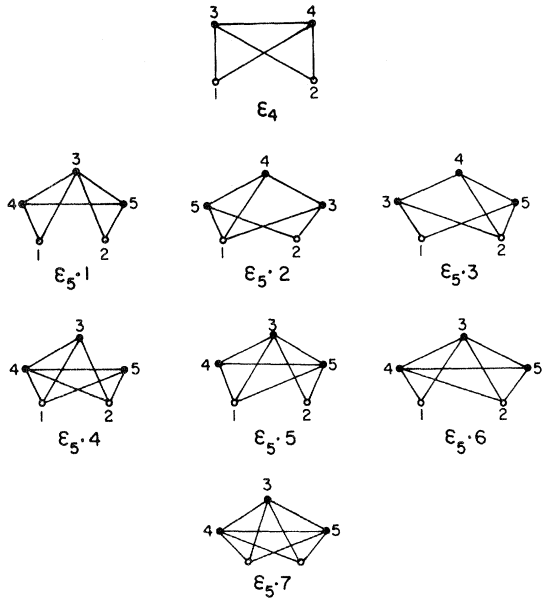

FIG. 1. The ϵ_4 and ϵ_5 elementary diagrams. The black dots and circles represent internal and external points, respectively. The lines represent $g-1$ links.

The three-particle distribution function $g_3(r_{12},r_{23},r_{31})$ is given by[6]

$$g_3(r_{12},r_{13},r_{23}) = g(r_{12})g(r_{23})g(r_{31}) \times \exp[A(r_{12},r_{23},r_{31})] \ , \quad (1.6)$$

where $A(r_{12},r_{23},r_{31})$ is the sum of so-called Abe diagrams. These Abe diagrams can also be expanded in a series

$$A = A_4 + A_5 + A_6 \cdots \ . \quad (1.7)$$

A_n and ϵ_n include all elementary diagrams that contribute to the HNC/n level of approximation. The diagrams contributing to A_4 and A_5 are shown in Fig. 2, and A_4 is given by

$$A_4(r_{12},r_{23},r_{31}) = \rho \int [g(r_{14})-1][g(r_{24})-1] \times [g(r_{34})-1]d^3r_4 \ . \quad (1.8)$$

We note that ϵ_n diagrams can be obtained by adding $[g(r_{13})-1]$ and $[g(r_{23})-1]$ lines to A_n diagrams and integrating over $\vec{r}_3$.

It has been known that to obtain an accurate evaluation of the energy expectation value, with HNC equations and an optimized $f(r)$ having r^{-2} tail, one needs to sum the slowly converging series (1.4) of elementary diagrams.[7] Thus far only the lowest three terms of this series, corresponding to HNC/4, HNC/5, and HNC/6 approximations, have been calculated.[7] The higher terms of the series are too complex for numerical evaluation. In Ref. 7 the HNC/$n \gtrsim 7$ terms are summed with Padé approximation. It has also been suggested[8] that there is a certain universality due to which we may approximate the sum of elementary diagrams $\epsilon(r)$ in liquids such as charged Bose gas or ^{4}He with that in hard-sphere gas at an appropriate density. In this approach one assumes that $\epsilon(r)$ is only a function of some equivalent hard-sphere gas density ρ_{eq}, and not of the detailed shape of $f(r)$.

In the present work we propose to use another approximate property of $\epsilon(r)$ to calculate it. It appears from Fig. 5 of Ref. 7 that the successive contributions ϵ_4, ϵ_5, ϵ_6 to $\epsilon(r)$ from HNC/4, HNC/5, and HNC/6 diagrams are approximately proportional. This proportionality suggests a scaling equation

$$\epsilon(r) \sim (1+s)\epsilon_4(r) \ , \quad (1.9)$$

where $\epsilon_4(r)$ is the HNC/4 contribution to $\epsilon(r)$. This scaling property may not be very specific to the functions used in Ref. 5; for example, it is shown in Sec.

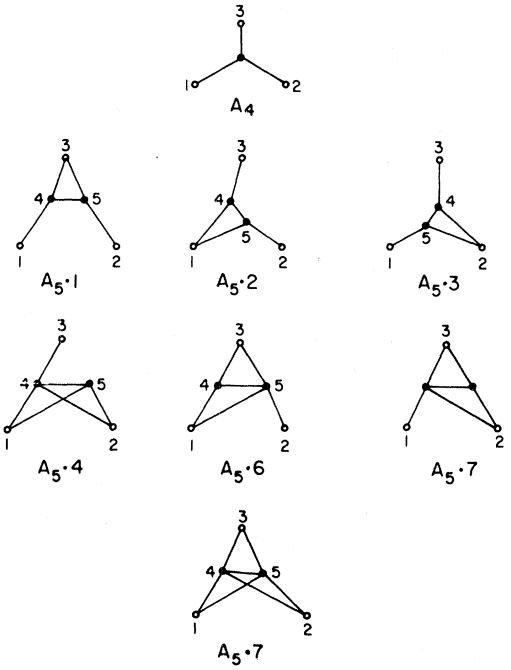

FIG. 2. The A_4 and A_5 diagrams in the Abe expansion of the three-body distribution function in terms of $g-1$ links.

II that an approximate scaling is obtained if the integrals contributing to ϵ_4 and ϵ_5 are calculated with Gaussian bonds. Studies of integrals contributing to A_n, with Gaussian bonds, suggest that $[\exp(A)-1]$ approximately scales with A_4, or

$$\exp[A(r_{12},r_{13},r_{23})]-1 \sim (1+s')A_4(r_{12},r_{13},r_{23}) \ , \quad (1.10)$$

and it is argued in Sec. II that the two scaling factors s and s' are related

$$s \sim 2s' \ . \quad (1.11)$$

Thus ϵ and A can be estimated from ϵ_4 and A_4 provided s is known.

The energy expectation value E can be written in different forms by integrating the kinetic energy terms by parts. The so-called Jackson-Feenberg (JF) energy[9] E_{JF} depends only upon the pair distribution function $g(r)$ and thus on the $\epsilon(r)$:

$$E_{JF} = \tfrac{1}{2}\rho \int g(r)\left\{v(r) - \frac{\hbar^2}{2m}\left[\frac{\nabla^2 f}{f} - \left[\frac{\nabla f}{f}\right]^2\right]\right\}d^3r \ . \quad (1.12)$$

The Pandharipande-Bethe (PB) energy depends upon both $g(r)$ and $g_3(r_{12},r_{13},r_{23})$, or equivalently on $\epsilon(r)$ and $A(r_{12},r_{23},r_{31})$:

$$E_{PB} = \tfrac{1}{2}\rho \int g(r)\left[v(r) - \frac{\hbar^2}{m}\frac{\nabla^2 f}{f}\right]d^3r - \frac{\hbar^2}{2m}\rho^2 \int g_3(r_{12},r_{23},r_{31})\frac{\vec{\nabla}_1 f(r_{12})}{f(r_{12})}\cdot\frac{\vec{\nabla}_1 f(r_{13})}{f(r_{13})}d^3r_2 d^3r_3 \ . \quad (1.13)$$

In general, at any HNC/n level of approximation [with Eqs. (1.4) and (1.7)], $E_{JF} \neq E_{PB}$,[10] however, $E_{JF} = E_{PB}$ in the limit $n \to \infty$. If we use the scaling Eqs. (1.9)–(1.11) for $\epsilon(r)$ and A the E_{JF} and E_{PB} are functions of the scaling variable s, and s is determined by requiring that

$$E_{JF}(s) = E_{PB}(s) \quad . \tag{1.14}$$

It was shown in Ref. 7 that $E_{PB} = E_{JF}$ follows from the Born-Bogoliubov-Green-Kirkwood-Yvon (BBGKY) relation between g and g_3. Thus, requiring Eq. (1.14) to hold would imply that the BBGKY relation is satisfied on average within the scaling approximation.

In Sec. III the proposed method, which we refer to as HNC/$\mathcal{S}$, is used to study the $E(\rho)$ and $g(r)$ in liquid ^{4}He with the McMillan correlation function.[11] There are extensive Monte Carlo calculations for this system, and it is shown that the $E(\rho)$, $g(r)$, and $\epsilon(r)$ obtained from the HNC/$\mathcal{S}$ equations are in essentially exact agreement with them. Results obtained with the HNC/$\mathcal{S}$ equations using the optimized correlation function are given in Sec. IV.

II. SCALING OF ϵ AND A

It is evident from Fig. 5 of Ref. 7 that ϵ_5 and ϵ_6 are approximately proportional to ϵ_4 and so $\epsilon_4 + \epsilon_5 + \epsilon_6$ can be approximated by $(1+s)\epsilon_4$. This scaling property may not be very sensitive to the detailed shape of $g-1$. Figure 3 shows ϵ_4 and ϵ_5 calculated with Gaussian approximation

$$g(r) - 1 = -\exp(-\pi\rho^{2/3} r^2) \quad , \tag{2.1}$$

chosen such that

$$\rho \int [1 - g(r)]\, d^3r = 1 \quad . \tag{2.2}$$

In this approximation[12] ϵ_4 and ϵ_5 can be analytically calculated

$$\epsilon_4(r) = -\frac{1}{32\sqrt{2}} \exp(-\alpha r^2) \quad , \tag{2.3}$$

$$\epsilon_5(r) = -\tfrac{1}{27}\{[(\tfrac{3}{7})^{3/2} - (\tfrac{9}{35})^{3/2}] \exp(-\tfrac{8}{7}\alpha r^2) + (\tfrac{3}{8})^{3/2} \exp(-\tfrac{7}{8}\alpha r^2) + [\tfrac{1}{6}(\tfrac{9}{50})^{3/2} - \tfrac{1}{2}(\tfrac{3}{10})^{3/2}] \exp(-\tfrac{3}{2}\alpha r^2)\} \quad , \tag{2.4}$$

where

$$\alpha = \pi\rho^{2/3} \quad .$$

It may be seen from (2.4) that the first and the second terms on the right-hand side within the square brackets would scale very well to $\epsilon_4(r)$, (2.3). The third term in (2.4), which does not scale to $\epsilon_4(r)$, is much smaller (by a factor ~ 5) compared to the other two terms and dies rapidly as r increases. Thus, overall ϵ_5 is quite proportional to ϵ_4. This scaling is evident from Fig. 3 where $\epsilon_5 \sim 0.58\epsilon_4$.

The A_4 and A_5 in the Gaussian approximation may be evaluated

$$A_4(r_{12}, r_{13}, r_{23}) = -(\tfrac{1}{3})^{3/2} \exp[-\tfrac{1}{3}\alpha(r_{12}^2 + r_{13}^2 + r_{23}^2)] \quad , \tag{2.5}$$

$$A_5(r_{12}, r_{13}, r_{23}) = -(\tfrac{1}{8})^{3/2} \mathcal{S} \sum \exp[-\alpha(\tfrac{1}{8}r_{12}^2 + \tfrac{1}{2}r_{13}^2 + \tfrac{1}{2}r_{23}^2)] + (\tfrac{1}{11})^{3/2} \mathcal{S} \sum \exp[-\tfrac{3}{11}\alpha(\tfrac{4}{3}r_{12}^2 + 3r_{13}^2 + \tfrac{4}{3}r_{23}^2)]$$
$$- (\tfrac{1}{15})^{3/2} \exp[-\tfrac{2}{3}\alpha(r_{12}^2 + r_{13}^2 + r_{23}^2)] \quad , \tag{2.6}$$

where the $\mathcal{S}\sum$ stands for the symmetrized sum over the indices 12, 13, and 23. Again, it is seen from Fig. 4 that A_5 scales with A_4, and $0.46A_4$ is a fairly good approximation of A_5.

We have merely shown above that ϵ_5 and A_5 differ from ϵ_4 and A_4 by mostly a scale factor. Of course this does not demonstrate the validity of approximations (1.9) and (1.10). However, it is shown in the next section that the results of Monte Carlo calculations are in agreement with Eq. (1.9). The results reported in Ref. 7 show that ϵ_6 also differs from ϵ_4 by a simple scale factor. All these together strongly indicate the plausibility of the scaling approximations (1.9) and (1.10).

It is necessary to have a relation between s and s' to use Eqs. (1.9) and (1.10) to estimate ϵ and A. We note that A_4 and ϵ_4 are related

$$\epsilon_4(r_{12}) = \tfrac{1}{2}\rho \int A_4(r_{12}, r_{13}, r_{23})[g(r_{13}) - 1] \times [g(r_{23}) - 1]\, d^3r_3 \quad , \tag{2.7}$$

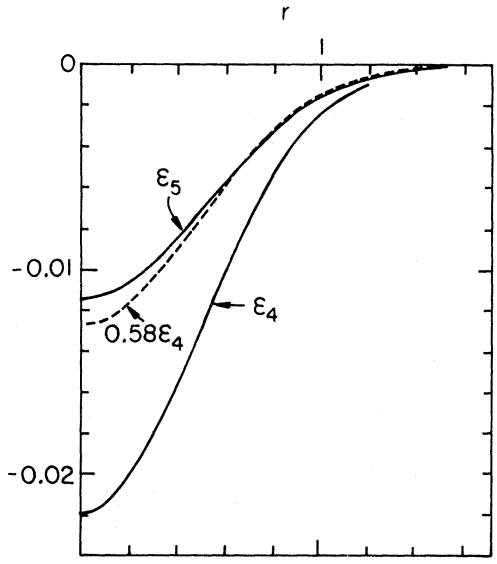

FIG. 3. The ϵ_4 and ϵ_5 elementary diagrams, in the Gaussian approximation, plotted as a function of r in units of r_0, where $r_0=(3/4\pi\rho)^{1/3}$.

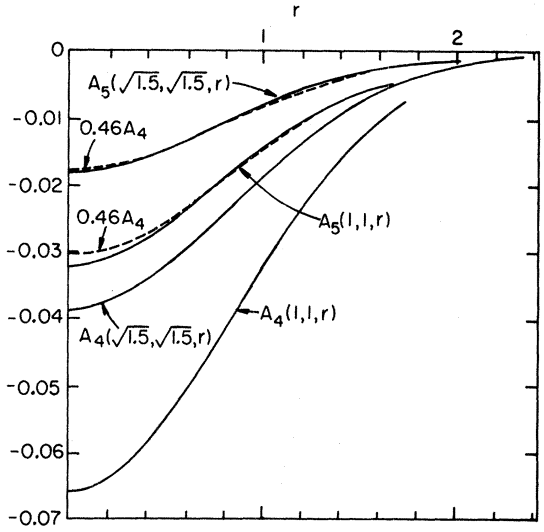

FIG. 4. The A_4 and A_5 diagrams in the Gaussian approximation plotted as a function of r in units of r_0 for the two choices $r_{12}=r_{13}=\sqrt{1.5}$ and $r_{12}=r_{13}=1$.

however, in general

$$\epsilon(r_{12}) \neq \rho \int A(r_{12},r_{13},r_{23})[g(r_{13})-1] \times [g(r_{23})-1]d^3r_3 \ . \tag{2.8}$$

In general ϵ_n diagrams can be obtained by adding $[g(r_{13})-1]$ and $[g(r_{23})-1]$ links to A_n diagrams and converting point 3 to an internal point. For example diagrams $\epsilon_5 \cdot 1$–7 of Fig. 1 can be constructed from diagrams $A_5 \cdot 1$–7 of Fig. 2 in this way. However, in ϵ_n diagrams the point 3 may be equivalent to an other. For example, 3 and 4 are equivalent in ϵ_4, while 3 and 5 are equivalent in $\epsilon_5 \cdot 2$ and $\epsilon_5 \cdot 3$. There are symmetry factors, such as the half in Eq. (2.7) associated with these symmetries, and (2.8) is not an equality due to the omission of these factors.

One would expect that the most important A_n diagrams are those that have the least number of $(g-1)$ bonds. Examples of such A_6 and A_7 diagrams are given in Fig. 5. The E_6 and E_7 diagrams generated from these have no symmetry factor associated with them and the following equality is valid for $n \geq 6$:

$$\epsilon_n'(r_{12}) = \rho \int A_n'(r_{12},r_{23},r_{31})[g(r_{13})-1][g(r_{23})-1]d^3r_3 \quad (n \geq 6) \ , \tag{2.9}$$

where A_n' and ϵ_n' denote contributions of the leading A_n and ϵ_n diagrams. Thus if we assume that the $A-A_4$ and $\epsilon-\epsilon_4$ are dominated by $A_{n\geq 6}'$ and $\epsilon_{n\geq 6}'$, and $A \ll 1$ so that $\exp(A)$ is $1+A$, we obtain

$$s\epsilon_4 = \sum_{n\geq 5} \epsilon_n \sim \rho \int \sum A_n [g(r_{13})-1][g(r_{23})-1]d^3r_3 \sim \rho s' \int A_4[g(r_{13})-1][g(r_{23})-1]d^3r_3 \sim 2s'\epsilon_4 \ , \tag{2.10}$$

and so expect $s \sim 2s'$.

TABLE I. The calculated energies (in K) and scaling factors s at various densities (in σ^{-3}).

ρ	0.330	0.350	0.365	0.38	0.401
PB/HNC	−6.66	−6.82	−6.91	−6.97	−7.00
JF/HNC	−5.11	−4.90	−4.67	−4.37	−3.84
HNC/*S*	−5.93	−5.91	−5.85	−5.75	−5.55
s.f.(s)	2.08	2.26	2.36	2.48	2.66

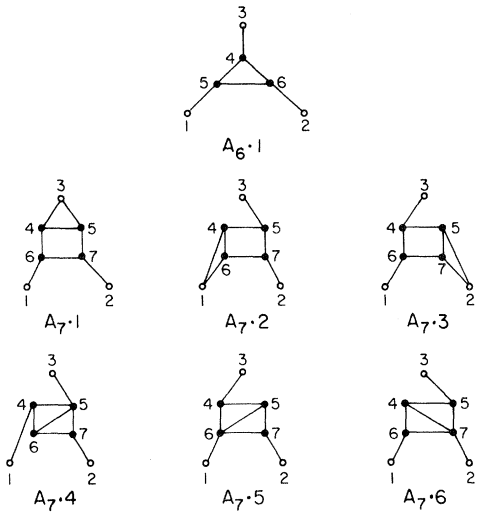

FIG. 5. The leading A_6 and A_7 diagrams.

The s may be somewhat less than $2s'$ due to the HNC/5 diagrams $\epsilon_5 \cdot 1-3$ and $A_5 \cdot 1-3$ for which Eq. (2.9) is not valid. $A_{n\geq 6}$ diagrams have ≥ 3 internal points, and their leading terms (having the least number of $g-1$ bonds) have the external points 1, 2, and 3 bonded to different points (as shown in Fig. 5). Thus when $\epsilon_{n\geq 6}$ diagrams are generated from these leading $A_{n\geq 6}$ diagrams, by adding $g(r_{13})-1$ and $g(r_{23})-1$ bonds and making 3 an internal point, no symmetry factor needs to be taken into account. Point 3 remains as the only point connected to both points 1 and 2. Unfortunately this is not true for the leading A_5 diagrams $A_5 \cdot 2$ and $A_5 \cdot 3$ (Fig. 2). The ϵ_5 diagrams $\epsilon_5 \cdot 2$ and $\epsilon_5 \cdot 3$ generated from these have equivalent points 3 and 5 (Fig. 1) and thus a symmetry factor $\frac{1}{2}$. Hence if we define s_5 and s_5' as

$$A_5 \sim s_5' A_4 \ , \tag{2.11}$$

$$\epsilon_5 \sim s_5 \epsilon_4 \ , \tag{2.12}$$

$s_5 \neq 2s_5'$. If diagrams $A_5 \cdot 4-7$ are negligible we expect $s_5 \sim 4s_5'/3$, and in numerical calculations (Figs. 3 and 4) we find $s_5 \sim 1.27 s_5'$.

The scaling factor s has a value around 2.3 (Table I) in ^{4}He liquid, of which we can expect only ~ 0.6 to come from ϵ_5. Hence, we can expect $\epsilon_{n\geq 6}$ to give the dominant contributions to ϵ, and therefore we have used $s = 2s'$ in most of the calculations. However, the results are not too sensitive to the assumed value of s/s'.

III. CALCULATIONS WITH McMILLAN CORRELATION FUNCTION

In this section we will describe the calculations and numerical results with a correlation function of the McMillan[11] form:

$$f(r) = \exp[-\tfrac{1}{2}(b/r)^5] \ , \tag{3.1}$$

with $b = 1.17\sigma$. This correlation function has been extensively used in the variational Monte Carlo studies of liquid ^{4}He. The calculations use Lennard-Jones potential (in K):

$$v(r) = 40.88[(\sigma/r)^{12} - (\sigma/r)^6] \ , \tag{3.2}$$

with $\sigma = 2.556$ Å.

Results of energy calculations, as a function of density, are shown in Fig. 6. The Monte Carlo points with larger error bars are taken from Ref. 13, whereas the points with smaller error bars are taken from Ref. 14. The spectacular success of HNC/$\mathcal{S}$ equations is evident. The lowest and topmost curves give the HNC energies in PB and JF forms, respectively. They are a way off from the Monte Carlo points. The next two curves labeled as HNC/4 give the two energies in the HNC/4 approximation. Again, they are seen to be quite away from the Monte Carlo points, however, the PB energies have a slight edge over the JF energies. The full HNC/$\mathcal{S}$ curve gives the energies calculated with the HNC/$\mathcal{S}$ equations. There is almost a complete overlap with the Monte Carlo points. The effect of not exponentiating the two-body elementary diagrams is also studied. The dashed HNC/$\mathcal{S}$ curve, which merges with the full curve at low densities, corresponds to the approximation

$$g_{\mathrm{HNC}/\mathcal{S}}(r) = f^2 e^{N(r)}[1 + (1+2s)\epsilon_4(r)] \tag{3.3}$$

instead of Eq. (2.2). The discrepancy between the

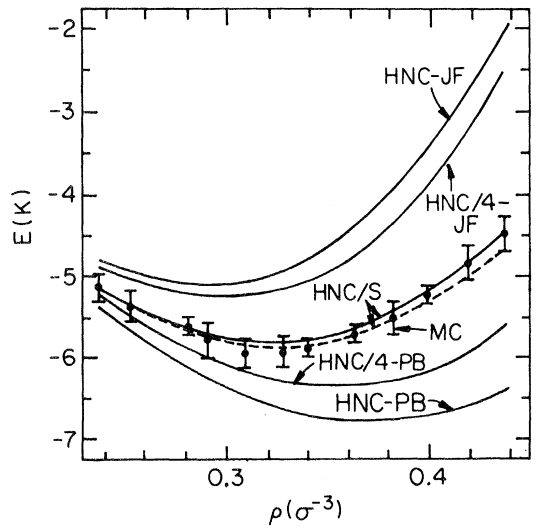

FIG. 6. Comparison of JF and PB energies in HNC, HNC/4, and HNC/$\mathcal{S}$ approximations with Monte Carlo results for the McMillan form of the correlation function.

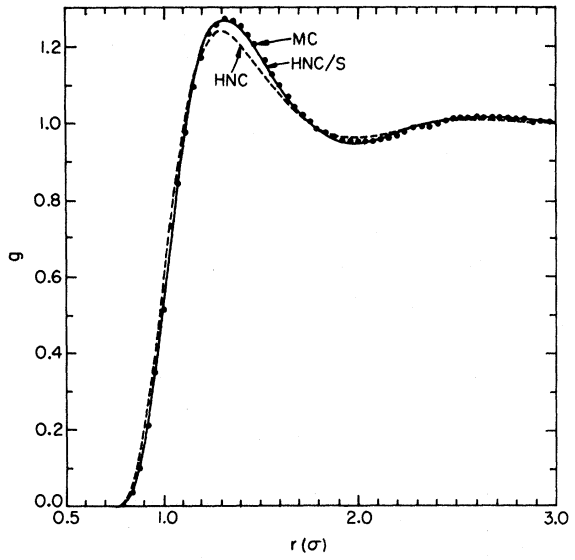

FIG. 7. The two-body distribution function at the equilibrium density $\rho=0.365\sigma^{-3}$. The Monte Carlo points are taken from Ref. 13.

two curves at higher densities and agreement of the full curve with Monte Carlo points suggests that the two-body elementary diagrams should be exponentiated.

In Fig. 7, we have plotted the distribution function, $g(r)$, in the HNC and HNC/$\mathcal{S}$ approximations at the equilibrium density $\rho=0.365\sigma^{-3}$. The full curve refers to HNC/$\mathcal{S}$ and the dashed curve refers to HNC. It may be seen that the agreement between

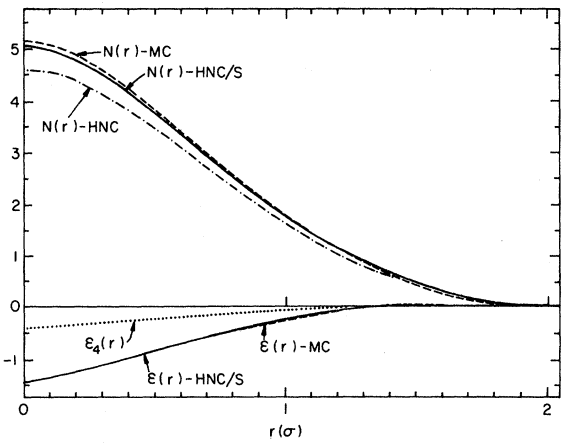

FIG. 8. Comparison of the contribution of nodal and elementary diagrams in the HNC/$\mathcal{S}$ approximation with the Monte Carlo results at the equilibrium density. The dot-dashed curve represents the HNC $N(r)$, and the dotted curve gives the $\epsilon_4(r)$. It is not possible to extract Monte Carlo $\epsilon(r)$ for $r<0.8\sigma$.

the HNC/$\mathcal{S}$ curve and Monte Carlo points is excellent in all the regions.

Next, using the Monte Carlo $g(r)$ and Eq. (2.3) we have calculated the Monte Carlo $N(r)$. This $N(r)$ is shown in Fig. 8 by a dashed curve. The full curve in Fig. 8 represents the HNC/$\mathcal{S}$ $N(r)$. The dot-dashed curve is HNC $N(r)$. Substituting the Monte Carlo $N(r)$ into (2.2) we calculate the Monte Carlo $\epsilon(r)$ shown by a dashed curve in Fig. 8. The full curve is HNC/$\mathcal{S}$ $\epsilon(r)$ and dotted curve is $\epsilon_4(r)$. As expected the HNC/$\mathcal{S}$ and Monte Carlo $\epsilon(r)$ are almost identical.

We carried out the energy calculations at the equilibrium density assuming $s=1.4s'$ instead of $2s'$. This changes the energy from -5.7 to -5.6 K. Thus, the results are not too sensitive to the assumed ratio of s to s'. Nevertheless, $s=2s'$ is both theoretically plausible, and gives essentially the Monte Carlo results.

IV. CALCULATIONS WITH OPTIMIZED CORRELATION FUNCTION

For the boson systems, a relative two-body Schrödinger type equation

$$\left[-\frac{\hbar^2}{m}\nabla^2+v(r)+\omega(r)\right]\sqrt{g(r)}=0 \tag{4.1}$$

for $g(r)$ has been obtained by making the energy stationary with respect to variations of $f(r)$.[7,15] Here, $\omega(r)$ is an induced potential given by

$$\omega(r)=\omega_0(r)+\frac{\hbar^2}{4m}\left[\nabla^2\epsilon(r)+2\frac{\delta\epsilon}{\delta g}\right], \tag{4.2}$$

with

$$\omega_0(r)=\frac{\hbar^2}{4m}\nabla^2\left[3N(r)-\rho\int N(r')(g-1-N)_{r-r'}\,d^3r'\right]. \tag{4.3}$$

In Eq. (4.2) the term within the parentheses is much smaller[5] than $\omega_0(r)$, and its inclusion makes very small changes in the energy. We will, therefore, neglect it here and work in the approximation $\omega(r)\sim\omega_0(r)$.

The properties of Eq. (4.1) have been studied in detail in Ref. 15, where an iterative procedure was employed for its solution. However, the convergence of this procedure depends very sensitively upon the input choice of correlation function $f(r)$. We have employed a different procedure for the solution of Eq. (4.1) in which the initial choice of $f(r)$ is not too important. We solve Eq. (4.1) up to some distance $d(=2$ to $3\sigma)$, much smaller than the one employed in Ref. 15, and match the resulting $f(r)$ with the asymptotic $f(r)$ at $r=d$

$$f(r\geq d)=1-\alpha/r^2\ ,\quad f'(r\geq d)=2\alpha/r^3\ , \tag{4.4}$$

where

$$\alpha = \frac{mc}{2\pi^2\rho\hbar} \ , \tag{4.5}$$

and c is the sound velocity. The matching is achieved by adding a variable parameter λ to the induced potential (4.3). This λ may also take into account the neglected term in Eq. (4.2). Equation (4.1) now becomes

$$\left[-\frac{\hbar^2}{m}\nabla^2 + v(r) + \omega_0(r) + \lambda\right]\sqrt{g(r)} = 0 \ , \tag{4.6}$$

for $r \leq d$.

We now give a brief outline of our procedure. Assume a value for the velocity of sound c. Take some arbitrary $f(r)$ whose value and derivative matches with (4.4) at $r = d$. Obtain the initial $g(r)$ from the HNC equations

$$g(r) = f^2(r)e^{N(r)} \ ,$$
$$N(r_{12}) = \rho \int [g(r_{13}) - 1][g(r_{23}) - 1 - N(r_{23})]d^3r_3 \ . \tag{4.7}$$

This $g(r)$ and $N(r)$ are used to calculate $\omega_0(r)$ from (4.3). The $\omega_0(r)$ may now be substituted into (4.6) to obtain a new $g_n(r)$. The parameter λ is varied so that the new $f(r)$ given by

$$f_n(r) = \sqrt{g_n(r)}\exp[-N(r)/2] \tag{4.8}$$

and its derivative matches with (4.4) at $r = d$. The $f_n(r)$ with its asymptotic form (4.4) is used in Eq. (4.7) to get the $g(r)$ and $N(r)$ in the entire region for the next iteration. This procedure is iterated till self-consistency is achieved. We note that the elementary diagram contribution $\epsilon(r)$ is neglected in this calculation of the optimum $f(r)$. The $\epsilon(r)$ has probably little effect on the $f(r)$.[7]

The optimum $f(r)$ is then used to calculate the energy with the HNC/$\mathcal{S}$ equations. The calculations are done at a number of densities, and a new value of the sound velocity c is obtained from the relations

$$P(\rho) = \rho^2\frac{\partial E(\rho)}{\partial\rho} \ , \quad c(\rho) = \left[\frac{1}{m}\frac{\partial P(\rho)}{\partial\rho}\right]^{1/2} \ , \tag{4.9}$$

where P is pressure. Using these values of $c(\rho)$ we start again iterating from (4.4). However, in the present calculations the $c(\rho)$ converged in just two iterations.

In our calculation we varied d from 1.5 to 3σ. After 2σ the energies were found to be insensitive to d. Thus, in all our calculations we have taken $d = 2\sigma$. The value of λ at this d was $\sim$0.5 K which decreased to $\sim$0.05 K at $d = 3\sigma$. The results with the optimized $f(r)$ at various densities are given in Table I. The second and the third rows give the HNC energies in PB and JF formats. At the equilibrium density we obtain the HNC/$\mathcal{S}$ energy -5.85 K which compares well with the best variational Monte Carlo[2] value -5.94 ± 0.03 K and the value -5.77 K obtained by Smith *et al.*[7] The last row gives the scaling factor s at various densities as determined from HNC/$\mathcal{S}$ equations.

In Table II we give sound velocities in HNC and HNC/$\mathcal{S}$ approximations and compare them with GFMC[1] and experiment.[16] These velocities were calculated by making a second-degree polynomial fit to $E(\rho)$ and using relations (4.9). It may be seen that the JF and PB sound velocities differ widely from each other. However, like the energies, they bracket the HNC/$\mathcal{S}$ sound velocities. The HNC/$\mathcal{S}$ velocities are seen to be closer to experimental and GFMC values. Hopefully, the remaining discrepancy would be bridged, to a considerable extent, by introducing three-body correlations in the wave function.

Lastly, we have calculated the liquid structure function $S(k)$ and compare it with experiment in Fig. 9. The experimental data are taken from Refs. 17

TABLE II. Sound velocities in m/s.

ρ	HNC		HNC/$\mathcal{S}$	GFMC	Expt.
	JF	PB			
0.330	274	131	194	. . .	. . .
0.350	304	155	217	. . .	. . .
0.365	325	172	235	245.8 ±21	238.2
0.380	347	188	252	264.7 ±14.9	266.4
0.401	377	211	275	290.54 ±8.74	306.2

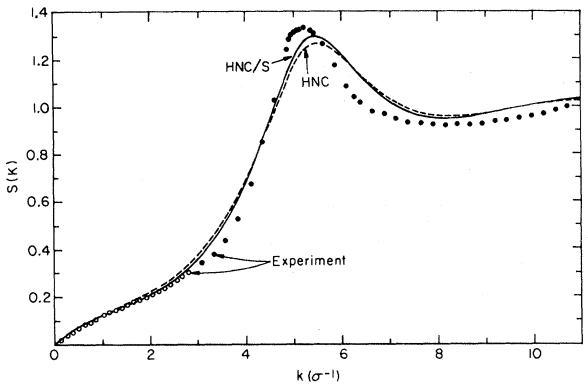

FIG. 9. The liquid structure function, $S(k)$, in HNC and HNC/s approximations.

and 18. The calculated $S(k)$ is linear and compares well with the data in the low momentum transfer region. Because of (4.4), it goes exactly to zero at $k=0$ as it should. In the regions of maximum and minimum of $S(k)$ the HNC/s works better than HNC, but we believe that three-body correlations may improve the situation considerably.

V. CONCLUSION

The scaling method and calculations presented in previous sections demonstrate that the series of elementary diagrams may be summed in a simple and reliable way. Two basic assumptions are involved. Firstly, the ϵ and A scale to ϵ_4 and A_4, respectively, and secondly, the two scaling factors are related to each other through the relation $s=2s'$. These assumptions are made plausible and their validity is best demonstrated by comparing the results of HNC/s equations with the Monte Carlo calculations.

The logical extension of the present work would be to incorporate three-body correlation functions in the wave function.[2,3] Scaling equations for the elementary diagrams containing the three-body correlation functions can be obtained. Calculations on these lines are in progress.

ACKNOWLEDGMENTS

The authors are thankful to Dr. S. Fantoni for many helpful discussions. This work was supported by the NSF under the MRL Grant No. DMR-80-20250 and the U.S. Department of Energy Contract No. DE-AC02-76ER01198.

*On leave from Department of Physics, AMU, Aligarh, India.

[1]P. A. Whitlock, D. M. Ceperley, G. V. Chester, and M. H. Kalos, Phys. Rev. B 19, 5598 (1979).
[2]K. Schmidt, M. H. Kalos, Michael A. Lee, and G. V. Chester, Phys. Rev. Lett. 45, 573 (1980).
[3]V. R. Pandharipande, Phys. Rev. B 18, 218 (1978).
[4]E. Feenberg, *Theory of Quantum Fluids* (Academic, New York, 1969); K. E. Schmidt and V. R. Pandharipande, Phys. Rev. B 21, 3945 (1980); C. E. Campbell and F. J. Pinski, Nucl. Phys. A328, 210 (1979).
[5]J. M. J. Van Leeuwen, J. Groeneveld, and J. DeBoer, Physica 25, 792 (1959).
[6]R. Abe, Prog. Theor. Phys. 21, 421 (1959).
[7]R. A. Smith, A. Kallio, M. Puoskari, and P. Toropainen, Nucl. Phys. A328, 186 (1979).
[8]Y. Rosenfeld and N. W. Ashcroft, Phys. Rev. A 20, 1208 (1979).
[9]H. J. Jackson and E. Feenberg, Ann. Phys. (N.Y.) 15, 266 (1961).
[10]V. R. Pandharipande and H. A. Bethe, Phys. Rev. C 7, 1312 (1973); V. R. Pandharipande and K. E. Schmidt, Phys. Rev. A 15, 2486 (1977).
[11]W. L. McMillan, Phys. Rev. 138, A442 (1965).
[12]R. A. Smith, Phys. Lett. 63B, 369 (1976).
[13]D. Schiff and L. Verlet, Phys. Rev. 160, 208 (1967).
[14]M. H. Kalos, D. Levesque, and L. Verlet, Phys. Rev. A 9, 2178 (1974).
[15]L. J. Lantto, A. D. Jackson, and P. J. Siemens, Phys. Lett. 68B, 311 (1977); A. D. Jackson, A. Lande, and L. J. Lantto, Nucl. Phys. A317, 70 (1979).
[16]P. R. Roach, J. B. Ketterson, and C. W. Woo, Phys. Rev. A 2, 543 (1970).
[17]E. K. Achter and L. Meyer, Phys. Rev. 188, 291 (1969).
[18]R. B. Hallock, Phys. Rev. A 5, 320 (1972).